Simultaneous multi-slice cardiac cine with Fourier-encoded self-calibration at 7 Tesla

Stanislas Rapacchi, Thomas Troalen, Zakarya Bentatou, Morgane Quemeneur, Maxime Guye, Monique Bernard, Alexis Jacquier, Frank Kober

Simultaneous Multi-Slice (SMS) cardiac cine with Fourier-encoded self-calibration at 7 Tesla

Stanislas Rapacchi[1,2], Thomas Troalen[3], Zakarya Bentatou[1], Morgane Quemeneur[1,2], Maxime Guye[1,2], Monique Bernard[1], Alexis Jacquier[1,4], Frank Kober[1]

1 Aix Marseille Univ, CNRS, CRMBM, Marseille, France

2 APHM, Hôpital Universitaire Timone, CEMEREM, Marseille, France

3 Siemens Healthineers, Paris, France

4 APHM, Hôpital Universitaire Timone, Radiology Dept, Marseille, France

Corresponding author:

Stanislas Rapacchi PhD

Aix Marseille Univ, CNRS, CRMBM

27 Bd Jean Moulin

Faculté de Médecine

13385 MARSEILLE CEDEX 05

+33 4 91 38 62 62

stanislas.rapacchi@univ-amu.fr

Word count: 3450

Running title: Self-calibrated SMS-cine at 7T

Keywords: Cardiac function MRI (cine), Simultaneous Multi-Slice (SMS), 7 Tesla cardiac magnetic resonance (CMR), Fourier encoding, ultra-high field MRI

Abstract

Purpose: To accelerate cardiac cine at 7T using simultaneous multi-slice (SMS) acquisition with self-calibration to solve for misalignment between calibration and imaging data due to breathing motion.

Methods: A spoiled-gradient echo cine sequence was modified with radiofrequency phase-cycled SMS excitations. A Fourier encoding strategy was applied along the cardiac phases dimension to allow for slice untangling and split-slice GRAPPA (SSG) calibration. SSG was coupled with regular GRAPPA (SMS-G) and L1-SPIRiT (SMS-L) for image reconstruction. SMS-3 cine was evaluated in ten subjects against single-slice (SS) cine in terms of signal and contrast-to-noise ratio (SNR, CNR) and slice leakage.

Results: SNR decreased significantly from 10.1 ± 7.1 for SS-cine to 7.4 ± 2.8 for SMS-3 cine with SMS-G ($p=0.02$), and was recovered to 9.0 ± 4.5 with SMS-L ($p=0.02$). CNR decreased significantly from 14.5 ± 8.1 for SS-cine to 5.6 ± 3.6 for SMS-3 cine with SMS-G ($p<0.0001$) and increased slightly but significantly back to 6.7 ± 4.4 for SMS-3 cine with SMS-L ($p=0.03$). SAR restrictions imposed a reduced nominal flip angle (-37±7%, $p=0.02$) for SMS excitations compared to SS acquisitions. SMS slice leakage increased significantly from apex (8.6 ± 6.5 %) to base (13.1 ± 4.1 %, $p=0.03$) in the left ventricle.

Conclusion: Three-fold acceleration of cine at 7T was achieved using proposed SMS technique. Fourier encoding self-calibration and regularized image reconstruction allowed to acquire three slices simultaneously without significant SNR decrease but a significant CNR decrease linked with reduced excitation nominal flip angle.

Introduction

7 Tesla (7T) MRI promises increased signal-to-noise ratio (SNR), which in cardiac MRI translates to a potential increase in imaging resolution for refined dynamic cardiac MRI (cine). Cine MRI is the fundamental of cardiac MRI that provides morphology, global and local function assessment, strain (1) and potentially even tissue characterization (2). Cine imaging resolution being highly anisotropic, one benefit from 7T cardiac MRI is to acquire thinner short-axis slices. However, thinner slices require more breath-holds to cover the entire ventricles. Numerous breath-holds would hamper a conventional MRI exam, as they are difficultly tolerated by patients and increase the possibility of misalignment of the stack of slices. To circumvent these issues**,** we propose to accelerate thin-slice cine MRI at 7T with a Simultaneous Multi-Slice (SMS) acquisition (3–5). SMS acquisitions enable to reduce the number of breath holds by the SMS acceleration factor employed (SMS-3 reduces the number of breath-holds by 3-fold). SMS acceleration corresponds to the excitation of multiple slices at the same time, coupled with a parallel imaging reconstruction that un-alias super-imposed images using the information from multi-elements receiver coil arrays.

SMS has already been applied to cine MRI at 7T by Schmitter et al(6), using parallel transmission and investigating the impact of triggering single-band calibration datasets for SMS reconstruction. In their work, calibration datasets were acquired with cardiac gating in a separate breath-hold. The synchronization in cardiac time between the calibration dataset and the aliased imaging dataset proved to significantly reduce cross-talk (i.e. leakage) between slices acquired simultaneously. SMS-cine was also demonstrated with balanced steady-state free precession (bSSFP) readout (7). The proposed SMS-cine technique allowed the acquisition of 2 slices simultaneously but the imposed shift in the frequency response was prone to artifacts for more than 2 slices. At 7T, due to larger static field inhomogeneity (B0) and SAR limitations, bSSFP is difficult to perform, thus spoiled gradient-echo (FLASH(8)) sequences are preferred for their robustness to B0 variations. As opposed to bSSFP, GRE sequences also impose less constraints on the conception of SMS strategies when more than two slices are to be acquired simultaneously. In this work, a custom SMS technique dedicated to high resolution GRE-cine imaging was implemented and evaluated at 7T in consideration of the application specificities but without parallel transmission.

First, SMS acquisitions require an excitation of multiple slices at the same time, which is achieved by multi-frequency bands excitation pulses. Since multi-band excitations deploy more power, they are necessarily limited by specific absorption rate (SAR) restrictions at 7T. Thus, the eventual cine image quality was evaluated as it depends on the achieved flip angle in the heart (9) and might therefore be impacted by SAR restrictions. Second, SMS reconstruction is conventionally calibrated from a separate non-aliased acquisition. Since cine acquisitions are performed under breath-hold, the calibration data have to be acquired either in a separate scan within the same breath-hold or with the same breath-hold position. Both would affect the quality and risk of corruption of the calibration data, the former due to low reproducibility across breath-holds and the latter due to prolongation of the breath-hold, which increases the risk of diaphragm drift. Interestingly, the first applications of SMS to cardiac imaging have been using Hadamard encoding(10,11) to boost image quality. The combination of multiple repetitions allowed obtaining each slice separately using Hadamard decoding. Following this concept, we propose here to exploit the redundancy in the cardiac temporal dimension to create an aliasing-free calibration dataset embedded in the imaging acquisition. Mimicking the Hadamard linear combination of multiple datasets, a cardiac-time Fourier encoding strategy was developed (12,13). The self-calibrated SMS cine acquisition was compared to the single-slice(SS) conventional cine. Finally, to alleviate the deteriorated image quality due to limited flip angle and noise amplification, a non-linear constrained image reconstruction was evaluated against conventional parallel imaging reconstruction.

Methods

Embedded calibration data using Fourier-encoding along the temporal dimension

Slice un-aliasing can be achieved using the CAIPIRINHA-SMS (5,14) technique, which facilitates this process by shifting their field-of-view and thus increasing the distance between superimposed voxels. CAIPIRINHA imposes that consecutive k-space lines observe incremental excitation phase that varies between slices to produce a linear phase increment across k-space. However, each acquired cardiac phase is independent of the others and provides a degree of freedom for extra phase modulation across cardiac phases. Therefore, an extra Fourier excitation

phase offset pattern was superimposed along the cardiac phase dimension (cardiac time dimension) for each k-space line to create a two-dimensional radiofrequency (RF) phase modulation. The complete RF excitation phase pattern is illustrated Figure 1 for 3 simultaneous slices (SMS-3). For SMS unwrapping, the reconstruction operates in three steps as follows: first, the Fourier phase offset decoding (i.e. Fourier transform) allows for combined cardiac phases to isolate k-spaces from each slice. For a SMS-N acceleration, the combination of N-phases is necessary. Multiple calibration datasets can then be embedded in the entire cine MRI dataset, with a total number of $N_{ref} = floor(N_{phase}/N_{SMS})$ calibration datasets with N_{phase} the number of complete cardiac phases and N_{SMS} the SMS acceleration factor. In this work, the N_{ref} calibration datasets are combined in a second step using singular value decomposition(SVD). As a third step, the first SVD eigenvector serves then for calibration of SMS reconstruction. In our case, Split-Slice-GeneRalized Autocalibrating Partial Parallel Acquisition (Split-Slice-GRAPPA, further noted SSG) (15,16) kernels (empirically optimized to a size of 3x3, see Supporting Information Figure S1) were calibrated over the cropped k-space center (32x24) with a Tikhonov regularization of 10^{-5}.

7T Cardiac MRI experiments

All experiments were performed on a 7T investigative human MRI scanner (Magnetom-7T Step 2.3, Siemens Healthcare GmbH, Erlangen, Germany), using a 32 receive(Rx)/8 transmit(Tx) channels coil (MRITools GmbH, Berlin, Germany) with the 8 Tx channels combined as a single channel with a hardware phase setting optimized for cardiac imaging. Transmit voltage calibration was performed using a vendor-provided calibration sequence. Within the considerations of B1+ field inhomogeneity from the use of transmit surface coils, a global nominal flip angle is still referenced per sequence to compare the relative effective RF power of each sequence.

This study was approved by the local Institutional Review Board in accordance with the guidelines outlined in the Declaration of Helsinki. Twelve healthy volunteers were enrolled in this study (6 women, 23±3 years old) after written consent was obtained. Due to the poor RF penetration from the concomitant use of transmit surface coils and limited RF power supply

(8kW), the subjects were recruited with a maximum body mass index (BMI) of 25 (avoiding overweight condition). SAR were limited to the initial level (Siemens "level 0") of established RF exposures.

A 2D FLASH-cine sequence with retrospective electrocardiogram gating was modified with CAIPIRINHA-SMS excitations (5) and the proposed cardiac time-Fourier RF phase cycling pattern. The radiofrequency (RF) pulses (1ms duration, time-bandwidth product 1.5) were then optimized for peak power using Wong's optimal phase offsets (17). Cine parameters were SMS-3 and GRAPPA-2 (24 auto-calibration lines), 1.8x1.8x4 mm^3 resolution reconstructed to 0.9x0.9x4 mm^3, 192x168 acquisition matrix, TE/TR = 2.56/5.0 ms, 28 ms temporal resolution, 501 Hz/pixel bandwidth, 75/256 asymmetrical echo and 2-fold readout oversampling, flow compensation in slice and read direction, ~10s breath-hold/acquisition. SMS slice distance was fixed to 20 mm. The same acquisitions were performed without SMS acceleration (noted single-slice or SS) for comparison. For both acquisitions, flip angles were maximized to fit within SAR restrictions and to obtain maximal FLASH-cine contrast-to-noise ratio (9,18). In order to strictly compare SS to SMS cine, additional SS acquisitions were matches to SMS in flip angle in four volunteers.

Image reconstruction

The image reconstruction was implemented in the Gadgetron (19) framework. A custom Matlab (Matlab R2017a, Mathworks, Natick, MA, USA) algorithm was designed as a "gadget" to perform our 3-steps SMS reconstruction: Fourier tranform, SVD and SSG. The in-plane reconstruction was then performed separately using gadgets available in the framework. Conventional GRAPPA (20) reconstruction was implemented for online reconstruction, further noted SMS-G. A second reconstruction using SSG + cardiac time-regularized L1-SPIRiT (21,22) was performed retrospectively for noise reduction, noted SMS-L. Asymmetrical echo and partial Fourier aspects were handled using a projection onto convex sets (POCS) reconstruction algorithm (23,24). Images were then interpolated with Gaussian k-space filtering. Eventually to facilitate visualization, a B1 filter was applied to the image series to correct for B1- gradient from the surface coil to the deep chest without affecting image contrast.

Image analysis

DICOM images were imported in Osirix for region-of-interest (ROI) based analysis. Signal-to-noise ratio (SNR) was evaluated as the mean-to-standard deviation ratio in a ROI drawn in the septum. SNR was measured at three levels: base, mid-ventricular and apex. Contrast-to-noise ratio (CNR) was evaluated as follows: the difference of mean intensity between the septum ROI and a ROI drawn over the left ventricle (LV) blood pool was then divided by the standard deviation of the septum ROI. The blood pool ROI was designed to avoid LV pillars. Slice leakage was evaluated by applying the corresponding SMS reconstruction (SMS-G) of the other two slices onto each of the three reconstructed slices (25). By crossing the SMS kernels of each slice onto the others allowed us to measure the residual signal that leaks between slices. The Split-Slice-GRAPPA reconstruction has been designed to minimize leakage at the kernel calibration level(15), so that applying the SMS kernels of slices 2 and 3 onto slice 1 should output minimal signal. Thus, leakage was defined as the sum of the signals measured in the two "leaked" slices over the signal of the original reconstructed slice. Since leakage comes primarily from SSG processing, only SMS-G was evaluated, similar leakage values being expected from SMS-L. Leakage was then measured using an ellipsoid ROI over the left ventricle.
Eventually for visualization purposes, the stack of short-axis slices was imported in Matlab and interpolated to an isotropic resolution for long axis view rendering using a 3D linear interpolation.
To evaluate the capacity of SMS-cine images to assess cardiac function locally, one expert radiologist with more than 25 years of experience in cardiac MRI was asked to rate each AHA sector(26) from 0 (no visibility of both endo and epicardium) to 5 (perfect assessment of local myocardium and its contractility).

Statistical analysis

All results were reported in Excel sheets (Microsoft, Redmond, WA, USA). Data were then compiled in JMP (SAS, Cary, NC, USA) for a pair-wise analysis of variance with Bonferroni post hoc test for normally distributed data and Kruskal-Wallis test analysis with Dun-Bonferroni

post hoc test for non-normally distributed data. A p-value inferior to 0.05 was considered statistically significant.

Results

SAR limited multi-band excitations penalize image quality

Figure 2 shows an example of a SMS-3 short-axis cine-FLASH acquisition compared with single slice acquisitions from the same locations. Conventional SS-cine provides excellent image quality for a 7T scan with homogeneous intensity over the heart except for a small B1+ void close to the anterior junction. The homogeneity of the heart's intensity is maintained using SMS-3 cine. Using 1ms 3-band excitations, specific absorption rate (SAR) restrictions required us to reduce the flip angle for SMS-3 cine by 38 ± 7% compared to single-band cine, i.e. from 36-69 to 20-50 degrees. We note that in both cases, the actual flip angle in the heart is likely to be lower than this nominal flip angle due to the inhomogeneous B1+ field. Additionally, SMS-3 images have increased noise, as measured by the difference of SNR in the septum from SS acquisitions to SMS acquisition (SNR(SS) = 9.9 ± 6.4 vs SNR(SMS-G) = 7.4 ± 2.8, p = 0.03). SNR decreased from apex to base due an increased distance from the transmit/receive surface coil, although differences were not significant.

Figure 3 illustrates a case of exacerbated signal variations due to the SAR-limited flip angle of multi-band excitations in one of the larger subjects of this study, and the benefits from regularized image reconstruction. With SMS, the LV wall of the basal slice was difficult to separate from the blood pool due to low effective flip angle and high noise level. The apical and mid-ventricular slices were closer to the surface coil and did not suffer from signal loss as much as the basal slice, distant from the coil. CNR decreased when using SMS acquisitions as shown in Figures 2 and 3. The CNR between the LV blood pool and the septum was significantly decreased from SS cine: CNR(SS)= 14.3 ± 7.7 to CNR(SMS-G)=5.6 ± 3.6 ($p<0.001$) for SMS-3-cine. Several effects participate in this image quality degradation: first, the limited SMS nominal flip angle reduced signal saturation difference between myocardium and fresh spins from flowing blood, in particular as the myocardium T1 is elongated at 7T (27); and second, noise was amplified by the SMS acceleration.

The influence of flip angle on CNR was verified when comparing SS, SMS-G and SS using matched flip angle (further noted SSmatched), as observed in Figure 4. There was very little differences in SNR between SS, SSmatched and SMS-G (11.0±6.5, 9.6±2.5 and 8.4±1.6 respectively). However there was a notable decrease of CNR between SS and both SSmatched and SMS-G (14.5±7.9 compared to 6.6±2.1 and 6.2±2.2 respectively, p(SS/SSmatched)=0.08 and p(SS/SMS-G)=0.05). These differences demonstrated flip angle has little impact on SNR but a strong influence on FLASH-cine CNR, as demonstrated previously by Tyler et al.(9)

Constrained reconstruction can reduce SMS noise amplification

Exploiting the sparsity in the spatio-temporal domain, SMS-L image reconstruction allowed to mitigate the noise amplification from SMS acquisition. Both SNR and CNR (Figures 3 and 5) were enhanced without compromising the morphological features and the peak systole analysis. The SNR was improved by 23 ± 36% (SNR(SMS-G)=7.5 ± 2.8 vs SNR(SMS-L)=9.4 ± 5.0, p=0.004) and the CNR was improved as well by 45 ± 25 % (CNR(SMS-G)=5.6 ± 4.0 vs CNR(SMS-L)= 7.3 ± 6.0, p=0.008). However, areas of low intensity tended to be shadowed even further by the regularization, as observed in the posterior wall and the abdominal organs bellow (Figure 4).

Figure 6 summarizes SNR and CNR variations, as measured at the three levels of the heart. The SNR loss from noise amplification due to SMS acceleration was compensated by constrained image reconstruction. However, the loss of CNR using multi-band excitations remained a penalty despite a significant improvement using regularized image reconstruction. Basal slices, further distant from the coil, suffered from a significantly lower CNR in both SS-cine (compared to both apical(p=0.01) and middle slices(p=0.02)) and SMS-3 cine using SMS-L (compared to apical slices, p=0.01).

Cardiac SMS-3 cine has limited leakage

Slice leakage was limited below 20% in the left ventricle using SMS-3 cine. Figure 7 illustrates leakage measured in the three slices. Average leakage increased significantly from apex (7.4±6.1%) to mid-ventricle (9.3±4.6%, p=0.02) and from mid-ventricle to base (12.0±4.7%,

p=0.02). Finally, the longitudinal spatial resolution can be appreciated by the reformat of the short-axis slices along the long axis of left ventricle, as demonstrated in Figure 8.

Evaluation of local cardiac function remains limited with SMS-cine

Figure 9 shows the mean ratings of local cardiac function and myocardium wall visualization for each of the 16 LV segments for the three techniques. Depending on the distance from the surface coil, the mid-ventricular and basal slices were difficult to assess, particularly for the posterior wall. The regularization from SMS-L significantly improved quality scores (from 3.6(SMS-G) to 3.9(SMS-L), $p<0.001$), despite not allowing full recovery of the contrast necessary for proper local myocardium evaluation that was obtained with SS-cine.

Discussion

This study demonstrates the feasibility and benefits of acquiring Simultaneous Multi-Slice dynamic cardiac MRI (SMS-cine) at 7 Tesla. The specificity of cardiac cine imaging was exploited to propose several improvements to SMS cine: first, the Fourier-encoding strategy allowed for embedded calibration data that circumvent issues with conventional separated single-slice calibration data; second, the sparsity along the cardiac time domain allowed for a constrained image reconstruction that mitigates the noise amplification from SMS acquisition.
As observed in this study, the benefits of extended spatial coverage from SMS acquisitions comes with the penalty of extra RF power that, in conjunction with strong SAR limitations at ultra-high field, directly impacts the ability to manipulate magnetization. In the context of cine, this drawback increases steady-state signal of static spins (i.e. myocardium) while decreasing signal of moving spins (i.e. flowing blood). The consequence is a partially recovered myocardium SNR and a severely decreased myocardium-blood CNR. Nonetheless, other applications such as phase-contrast MRI could benefit from SMS integration without penalization from the reduced RF power.
Two aspects of the proposed approach were not covered in this study: 1/ the benefits of integrating the calibration data into the imaging set rather than the conventional separate acquisition and 2/ the exploration of the multiple synchronous calibration datasets provided by

the self-calibrating strategy. First, Figure 10 shows an acquisition when the separate calibration was acquired at the beginning of each breath-hold. In our experience, this strategy led to calibration data misregistered to the imaging dataset. Indeed, we found that, without specific instructions or extra delay, volunteers did not reach their breath-hold at the beginning of the acquisition, such that SMS acquisition with separate calibration could not be exploited. Second, the self-calibration strategy provided between 4 and 7 calibration datasets depending on the subject heart rate. However, these calibration datasets were noisy when taken individually. As a consequence, the use of synchronous calibration datasets did not permit to properly perform the SMS reconstruction, as shown in Supporting Information Figure S2. We opted for the SVD for combining these datasets, which significantly reduced the noise level of the eventual calibration dataset. Additionally, the combination of different cardiac phases can be tolerated for SMS unwrapping given that the distance between overlapping pixels remains greater than the deformation induced by cardiac motion. Indeed, while cardiac motion spans deformations on the order of 1cm, the overlapping pixels have a distance defined by the CAIPIRINHA shift ($1/6^{th}$ of the phase FOV) and the slices gap (16mm). In this study, this distance is greater than 4cm, thus much larger than potential cardiac deformations.

Several aspects in the design of this study could be explored for further improvement. First, the benefits of SMS cine were explored with relatively thin slices (4mm thick) and a high in-plane resolution towards the purpose of high resolution cardiac MRI. In such severe conditions, the drawbacks of the proposed approach become blatant: strong noise amplification and loss of SNR and CNR are observed, and images loose diagnostic quality when heart's depth exceeded the penetration of the surface coil B1 fields (B1+ and B1-). Thicker slices could be acquired to provide sufficient signal from deep within the chest, and super-resolution techniques(28) could be integrated to achieve the sought high-resolution imaging. Second, image reconstruction was designed in a 2-step fashion, with SMS slice separation first (using split-slice GRAPPA) and phase-encode unwrapping second (GRAPPA or L1SPIRiT). An alternative would have been to perform a single-step image reconstruction(29,30), which could have helped better exploiting parallel imaging information in a 3D fashion. Adversely, the 2-step approach enables to balance between in-plane and through-plane noise amplification and residual artifact, and thus propose regularized algorithms such as L1-SPIRiT for phase-encode unwrapping. This ability to tune each reconstruction step can be critical to cardiac SMS-MRI as the coil arrangement is often not-

aligned with the slice orientations, which undermines the coil sensitivity variations between overlapping pixels. Third, it would be relevant to evaluate RF transmission through B1+ mapping (31) instead of reporting a nominal flip angle. Mapping the local variations of transmitted RF power would unveil the inhomogeneity of the B1+ field for tailored RF design and personalized SAR management. Unfortunately, sequences for cardiac B1+ mapping at 7T were not available on our system at the time of this study. Fourth and last, this study evaluated only SMS-3 acceleration. As observed in Supporting Information Figure S3, lower acceleration (SMS-2) allowed for improved image quality while higher acceleration (SMS-4) suffered from remaining aliasing artifacts and a lower nominal flip angle, which directly impacted the image quality. SMS-3 cine was chosen as a compromise between image quality and acceleration.

This study remains limited to a cohort of twelve healthy subjects for the purpose of demonstration. Additionally, the cardiac coil employed in this study was configured in a single transmit channel mode, despite presenting eight transmit channels. For simplicity, the eight channels were combined by a hardware pre-phaser, with a phase set optimized for cardiac imaging. While parallel transmit optimization (pTx) can certainly improve the B1+ field in the heart(22), the difficulty to measure and customize B1+ for shimming in the heart was beyond the scale of the current study. To circumvent severe B1+ penetration limitations, subjects were screened prior to recruitment for a limited BMI (<25). Even without pTx, several improvements could benefit SMS-cine: improved RF pulse design for reduced peak power (23) and more accurate slice separation (24) as well as variable-rate selective excitation (VERSE) pulse design (34).

Finally, SMS-cine was explored in this study with thinner slices mainly for cardiac function imaging, but it could also benefit to cardiac UHF-MRI with thicker slices to reduce acquisition time dedicated to cine and allow more examination time for novel UHF contrasts that require elongated acquisition durations, in particular for cardiac applications.

Conclusion

A novel SMS technique was proposed for SMS-cine acquisition at 7T. Exploiting cardiac cine specificity, Fourier encoded self-calibration and regularized image reconstruction allowed us to

acquire three slices simultaneously while maintaining SNR level. Nevertheless, due to SAR restrictions, the excitation flip angle had to be reduced from optimal values leading to significant CNR decrease using SMS-3 cine in the current experimental setting. This study therefore demonstrates general feasibility of SMS-cine but also illustrates its limitations, especially at ultra-high field.

Acknowledgements

This work was performed by a laboratory member of France Life Imaging network (grant ANR-11-INBS-0006), on the platform 7T-AMI, a French “Investissements d’Avenir” programme” (grant ANR-11-EQPX-0001).
The project leading to this publication has received funding from the following institutions: Excellence Initiative of Aix-Marseille University - A*MIDEX (grant ANR-11-IDEX-0001-02), a French “Investissements d’Avenir” programme”; Agence Nationale de la Recherche (grant ANR-14-CE17-0016); Fondation de la Recherche Médicale (grant FRM DBS20140930772).
Last but not least, the authors would like to thank Sebastian Schmitter and Giulio Ferrazzi for very insightful discussions.

References

1. Haig CE, McComb C, Berry C, Carrick D, Clerfond G, Gao H, Mangion K, Zhong X, Luo X. A Novel Method for Estimating Myocardial Strain: Assessment of Deformation Tracking Against Reference Magnetic Resonance Methods in Healthy Volunteers. Sci. Rep. 2016;6:38774. doi: 10.1038/srep38774.

2. Nordlund D, Kanski M, Jablonowski R, Koul S, Erlinge D, Carlsson M, Engblom H, Aletras AH, Arheden H. Experimental validation of contrast-enhanced SSFP cine CMR for quantification of myocardium at risk in acute myocardial infarction. J. Cardiovasc. Magn. Reson. 2017;19:12. doi: 10.1186/s12968-017-0325-y.

3. Barth M, Breuer F, Koopmans PJ, Norris DG, Poser BA. Simultaneous multislice (SMS) imaging techniques. Magn. Reson. Med. 2016;75:63–81. doi: 10.1002/mrm.25897.

4. Larkman DJ, Hajnal JV, Herlihy AH, Coutts GA, Young IR, Ehnholm G. Use of multicoil arrays for separation of signal from multiple slices simultaneously excited. J. Magn. Reson. Imaging JMRI 2001;13:313–317.

5. Breuer FA, Blaimer M, Mueller MF, Seiberlich N, Heidemann RM, Griswold MA, Jakob PM. Controlled aliasing in volumetric parallel imaging (2D CAIPIRINHA). Magn. Reson. Med. 2006;55:549–556. doi: 10.1002/mrm.20787.

6. Schmitter S, Moeller S, Wu X, Auerbach EJ, Metzger GJ, Van de Moortele P-F, Uğurbil K. Simultaneous multislice imaging in dynamic cardiac MRI at 7T using parallel transmission. Magn. Reson. Med. 2017;77:1010–1020. doi: 10.1002/mrm.26180.

7. Stäb D, Ritter CO, Breuer FA, Weng AM, Hahn D, Köstler H. CAIPIRINHA accelerated SSFP imaging. Magn. Reson. Med. 2011;65:157–164. doi: 10.1002/mrm.22600.

8. Haase A, Frahm J, Matthaei D, Hänicke W, Merboldt K-D. FLASH imaging: rapid NMR imaging using low flip-angle pulses. 1986. J. Magn. Reson. San Diego Calif 1997 2011;213:533–541. doi: 10.1016/j.jmr.2011.09.021.

9. Tyler DJ, Hudsmith LE, Petersen SE, Francis JM, Weale P, Neubauer S, Clarke K, Robson MD. Cardiac cine MR-imaging at 3T: FLASH vs SSFP. J. Cardiovasc. Magn. Reson. Off. J. Soc. Cardiovasc. Magn. Reson. 2006;8:709–715. doi: 10.1080/10976640600723797.

10. Müller S. Simultaneous multislice imaging (SIMUSIM) for improved cardiac imaging. Magn. Reson. Med. 1989;10:145–155.

11. Souza SP, Szumowski J, Dumoulin CL, Plewes DP, Glover G. SIMA: simultaneous multislice acquisition of MR images by Hadamard-encoded excitation. J. Comput. Assist. Tomogr. 1988;12:1026–1030.

12. Zhu K, Kerr A, Pauly JM. Autocalibrating CAIPIRINHA: Reformulating CAIPIRINHA as a 3D Problem. In: Proceedings of the 20th Annual Meeting of ISMRM. Melbourne, Australia; 2012. p. 518.

13. Zahneisen B, Poser BA, Ernst T, Stenger VA. Three-dimensional Fourier Encoding of Simultaneously Excited Slices: Generalized Acquisition and Reconstruction Framework. Magn. Reson. Med. Off. J. Soc. Magn. Reson. Med. Soc. Magn. Reson. Med. 2014;71:2071–2081. doi: 10.1002/mrm.24875.

14. Breuer FA, Blaimer M, Heidemann RM, Mueller MF, Griswold MA, Jakob PM. Controlled aliasing in parallel imaging results in higher acceleration (CAIPIRINHA) for multi-slice imaging. Magn. Reson. Med. 2005;53:684–691. doi: 10.1002/mrm.20401.

15. Cauley SF, Polimeni JR, Bhat H, Wald LL, Setsompop K. Interslice leakage artifact reduction technique for simultaneous multislice acquisitions. Magn. Reson. Med. 2014;72:93–102. doi: 10.1002/mrm.24898.

16. Setsompop K, Gagoski BA, Polimeni JR, Witzel T, Wedeen VJ, Wald LL. Blipped-controlled aliasing in parallel imaging for simultaneous multislice echo planar imaging with reduced g-factor penalty. Magn. Reson. Med. 2012;67:1210–1224. doi: 10.1002/mrm.23097.

17. Wong E. Optimized Phase Schedules for Minimizing Peak RF Power in Simultaneous Multi-Slice RF Excitation Pulses. In: Proceedings of the 20th Annual Meeting of ISMRM. Melbourne, Australia; 2012. p. 2209.

18. Gao JH, Holland SK, Gore JC. Nuclear magnetic resonance signal from flowing nuclei in rapid imaging using gradient echoes. Med. Phys. 1988;15:809–814. doi: 10.1118/1.596197.

19. Hansen MS, Sørensen TS. Gadgetron: an open source framework for medical image reconstruction. Magn. Reson. Med. 2013;69:1768–1776. doi: 10.1002/mrm.24389.

20. Griswold MA, Jakob PM, Heidemann RM, Nittka M, Jellus V, Wang J, Kiefer B, Haase A. Generalized autocalibrating partially parallel acquisitions (GRAPPA). Magn. Reson. Med. 2002;47:1202–1210. doi: 10.1002/mrm.10171.

21. Lustig M, Donoho D, Pauly JM. Sparse MRI: The application of compressed sensing for rapid MR imaging. Magn. Reson. Med. 2007;58:1182–1195. doi: 10.1002/mrm.21391.

22. Lustig M, Pauly JM. SPIRiT: Iterative self-consistent parallel imaging reconstruction from arbitrary k-space. Magn. Reson. Med. 2010;64:457–471. doi: 10.1002/mrm.22428.

23. Xu Y, Haacke EM. Partial Fourier imaging in multi-dimensions: A means to save a full factor of two in time. J. Magn. Reson. Imaging 2001;14:628–635. doi: 10.1002/jmri.1228.

24. Peng H, Sabati M, Lauzon L, Frayne R. MR image reconstruction of sparsely sampled 3D k-space data by projection-onto-convex sets. Magn. Reson. Imaging 2006;24:761–773. doi: 10.1016/j.mri.2005.12.028.

25. Xu J, Moeller S, Auerbach EJ, Strupp J, Smith SM, Feinberg DA, Yacoub E, Uğurbil K. Evaluation of slice accelerations using multiband echo planar imaging at 3 T. NeuroImage 2013;83:991–1001. doi: 10.1016/j.neuroimage.2013.07.055.

26. Cerqueira MD, Weissman NJ, Dilsizian V, Jacobs AK, Kaul S, Laskey WK, Pennell DJ, Rumberger JA, Ryan T, Verani MS. Standardized Myocardial Segmentation and Nomenclature for Tomographic Imaging of the Heart: A Statement for Healthcare Professionals From the Cardiac Imaging Committee of the Council on Clinical Cardiology of the American Heart Association. Circulation 2002;105:539–542. doi: 10.1161/hc0402.102975.

27. Rodgers CT, Piechnik SK, Delabarre LJ, Van de Moortele P-F, Snyder CJ, Neubauer S, Robson MD, Vaughan JT. Inversion recovery at 7 T in the human myocardium: measurement of

T(1), inversion efficiency and B(1) (+). Magn. Reson. Med. 2013;70:1038–1046. doi: 10.1002/mrm.24548.

28. Odille F, Bustin A, Chen B, Vuissoz P-A, Felblinger J. Motion-Corrected, Super-Resolution Reconstruction for High-Resolution 3D Cardiac Cine MRI. In: Medical Image Computing and Computer-Assisted Intervention – MICCAI 2015. Lecture Notes in Computer Science. Springer, Cham; 2015. pp. 435–442. doi: 10.1007/978-3-319-24574-4_52.

29. Koopmans PJ. Two-dimensional-NGC-SENSE-GRAPPA for fast, ghosting-robust reconstruction of in-plane and slice-accelerated blipped-CAIPI echo planar imaging. Magn. Reson. Med. 2017;77:998–1009. doi: 10.1002/mrm.26179.

30. Zhu K, Dougherty RF, Wu H, Middione MJ, Takahashi AM, Zhang T, Pauly JM, Kerr AB. Hybrid-Space SENSE Reconstruction for Simultaneous Multi-Slice MRI. IEEE Trans. Med. Imaging 2016;35:1824–1836. doi: 10.1109/TMI.2016.2531635.

31. Nehrke K, Börnert P. DREAM—a novel approach for robust, ultrafast, multislice B1 mapping. Magn. Reson. Med. 2012;68:1517–1526. doi: 10.1002/mrm.24158.

32. Wu F-H, Wu EL, Tung Y-H, Cheng P-W, Chiueh T-D, Chen J-H. A specific absorption rate reduction method for simultaneous multislice magnetic resonance imaging. Rev. Sci. Instrum. 2017;88:043701. doi: 10.1063/1.4979861.

33. Abo Seada S, Price AN, Hajnal JV, Malik SJ. Optimized amplitude modulated multiband RF pulse design. Magn. Reson. Med. 2017;78:2185–2193. doi: 10.1002/mrm.26610.

34. Conolly S, Nishimura D, Macovski A, Glover G. Variable-rate selective excitation. J. Magn. Reson. 1969 1988;78:440–458. doi: 10.1016/0022-2364(88)90131-X.

Figure captions

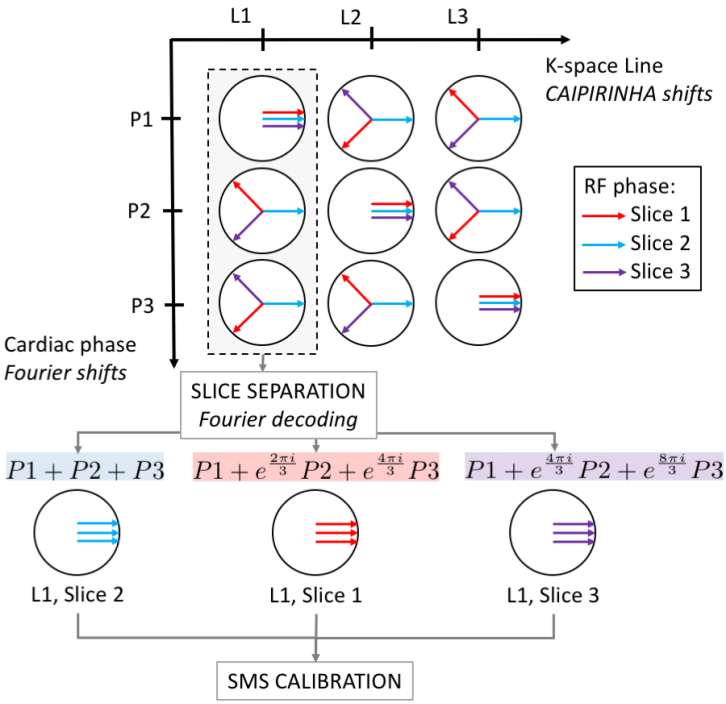

Figure 1: SMS-3-cine custom design of phase shifts encoding combining CAIPIRINHA phase shifts and Fourier encoded phase shifts along the cardiac phase dimensions. Proposed SMS-cine encoding provides embedded reference data for SMS calibration to perform slice separation.

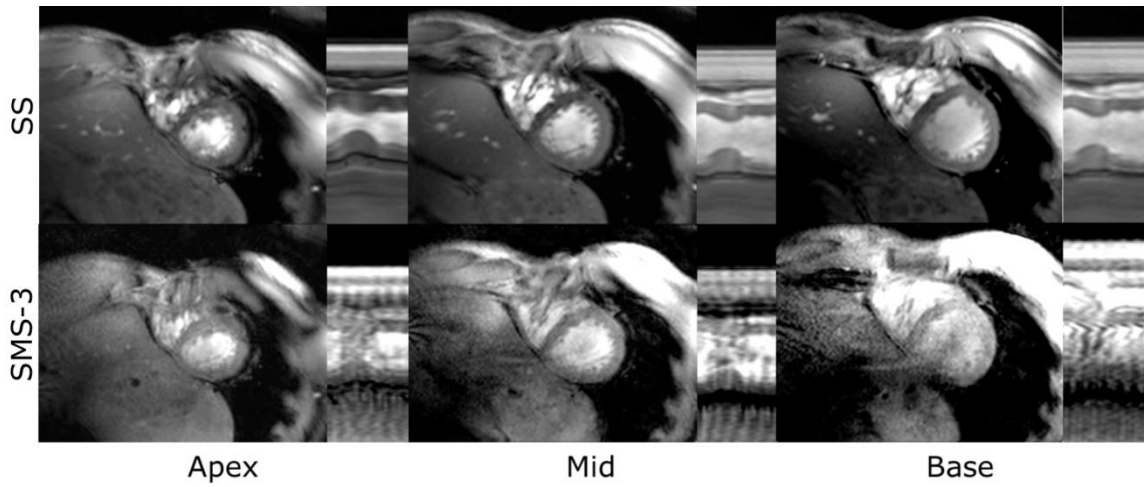

Figure 2: Examples of diastole images and y-t profiles from SMS-3 short-axis cine-FLASH compared with single slice acquisitions. The increased acceleration from SMS combined to the decreased flip angle due to SAR restrictions induced a loss of SNR and CNR between SS cine and accelerated SMS-3 cine. Losses increased from apex to base due to a greater distance from the surface coil. SMS-3 images were reconstructed with SMS-G.

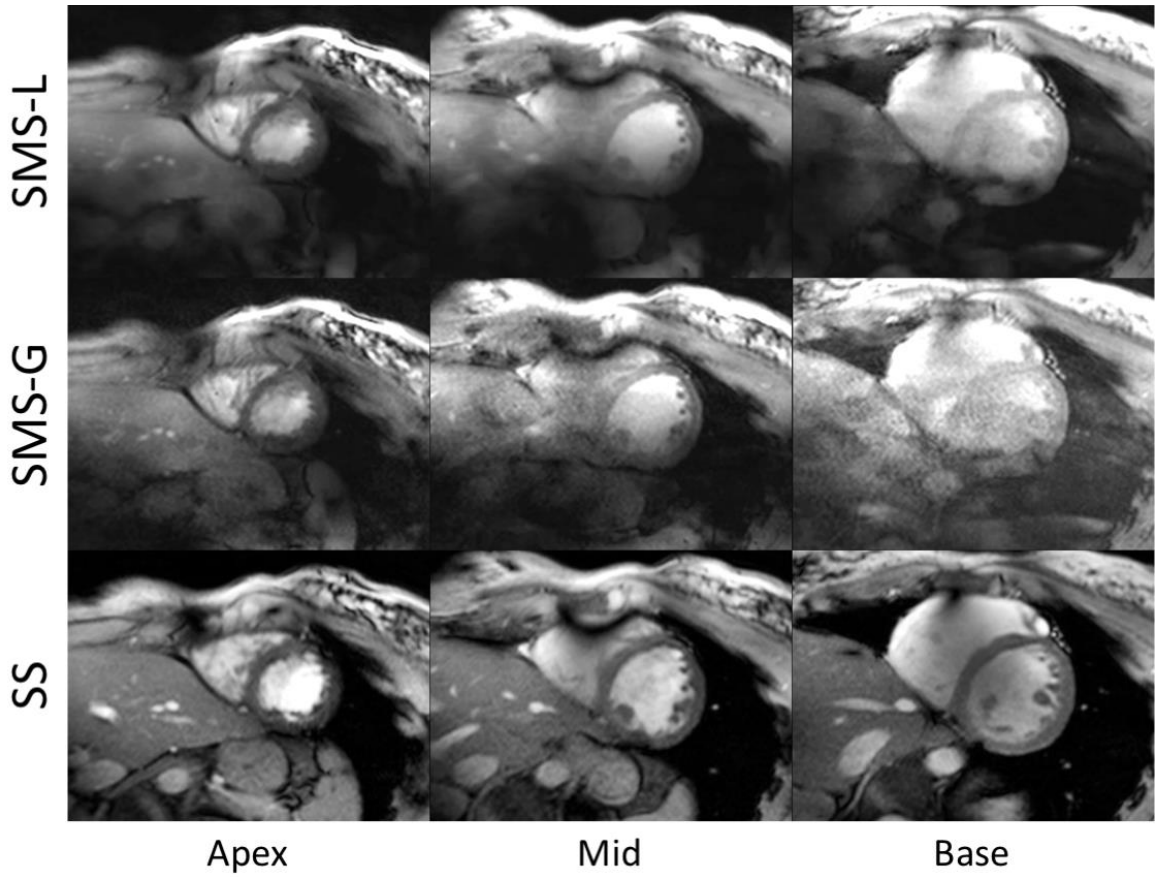

Figure 3: In the case of the heart being morphologically further away from the surface coil, a severe loss of SNR and CNR was observed between SS-cine and SMS-3-cine. Constrained image reconstruction (SMS-L) reduced noise amplification compared to SMS-G. Nominal flip angle instructions were 69° for SS and 40° for SMS-3. Dark spots in SMS-3-cine images are exacerbated B1+ losses.

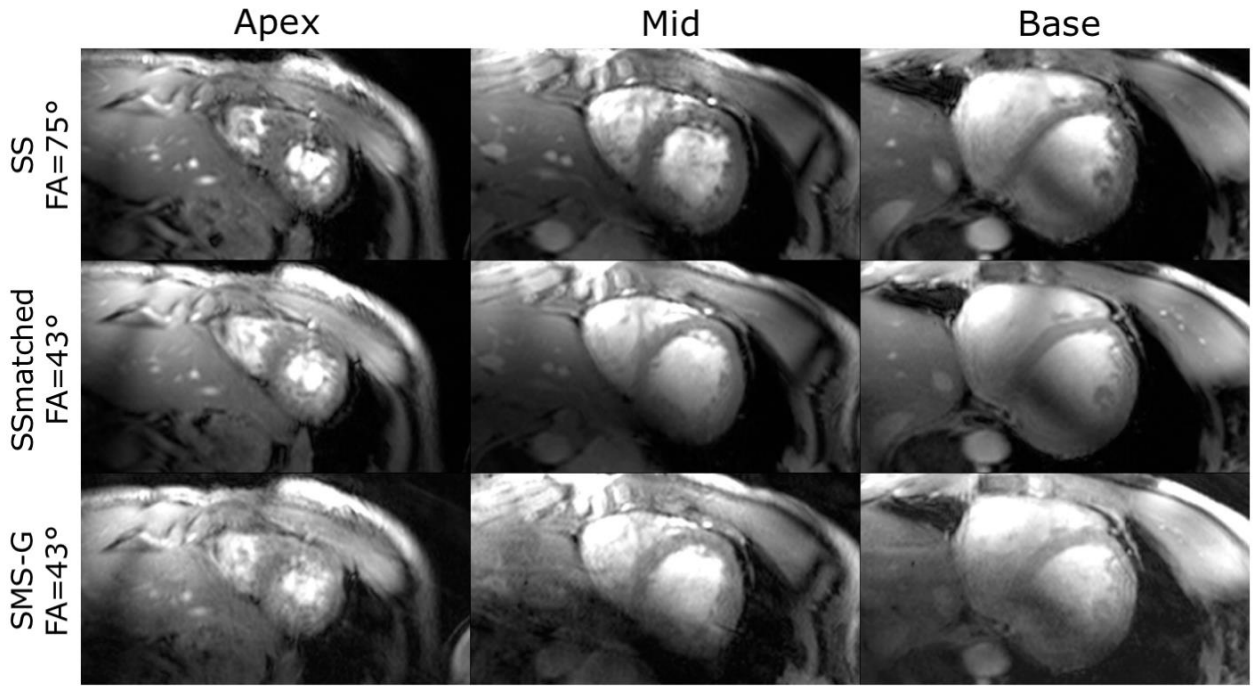

Figure 4: Comparison between SS and SMS-G at maximum SAR levels and SS with matched flip angle (SSmatched) with SMS. By decreasing the flip angle, the steady-state signal of static spins (myocardium) increases while the transient signal from flowing spins (blood) decreases. Consequently, the contrast between blood and myocardium decreases with the flip angle.

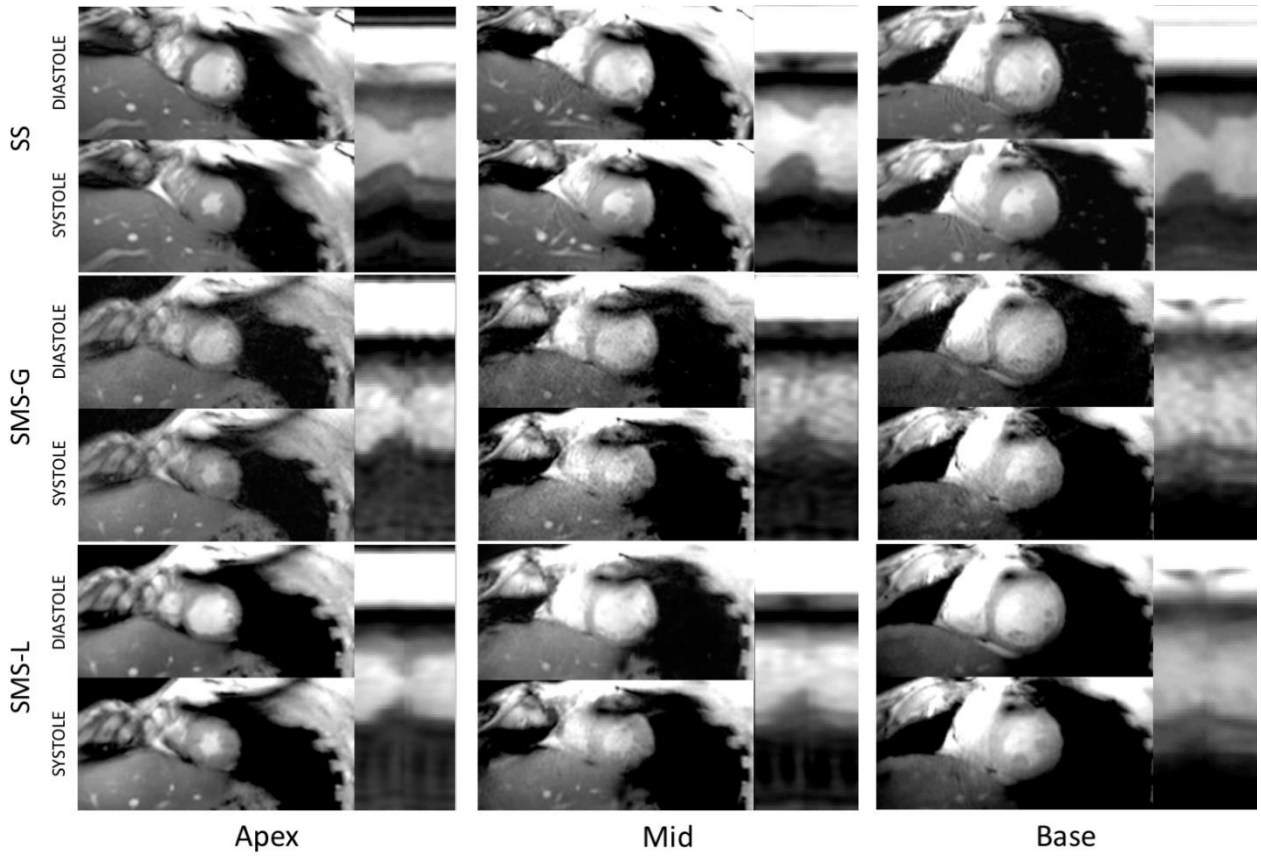

Figure 5: After split-slice GRAPPA (SSG), L1-SPIRiT non-linear regularized image reconstruction (SMS-L) improved the SNR and CNR compared to the conventional GRAPPA (SMS-G) reconstruction.

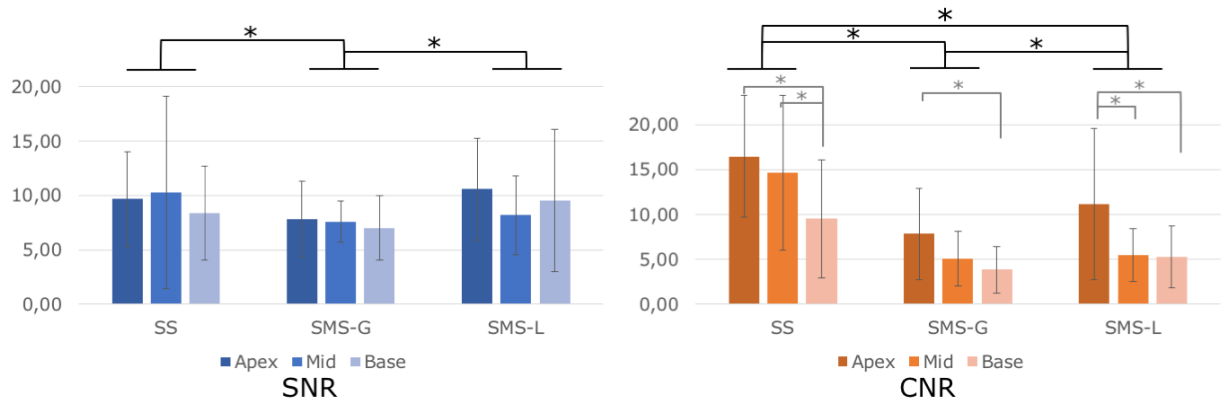

Figure 6: Bar graphs of SNR and CNR measurements at the three ventricle levels: apex, mid and base. Statistically significant differences ($p<0.05$) are noted with a *.

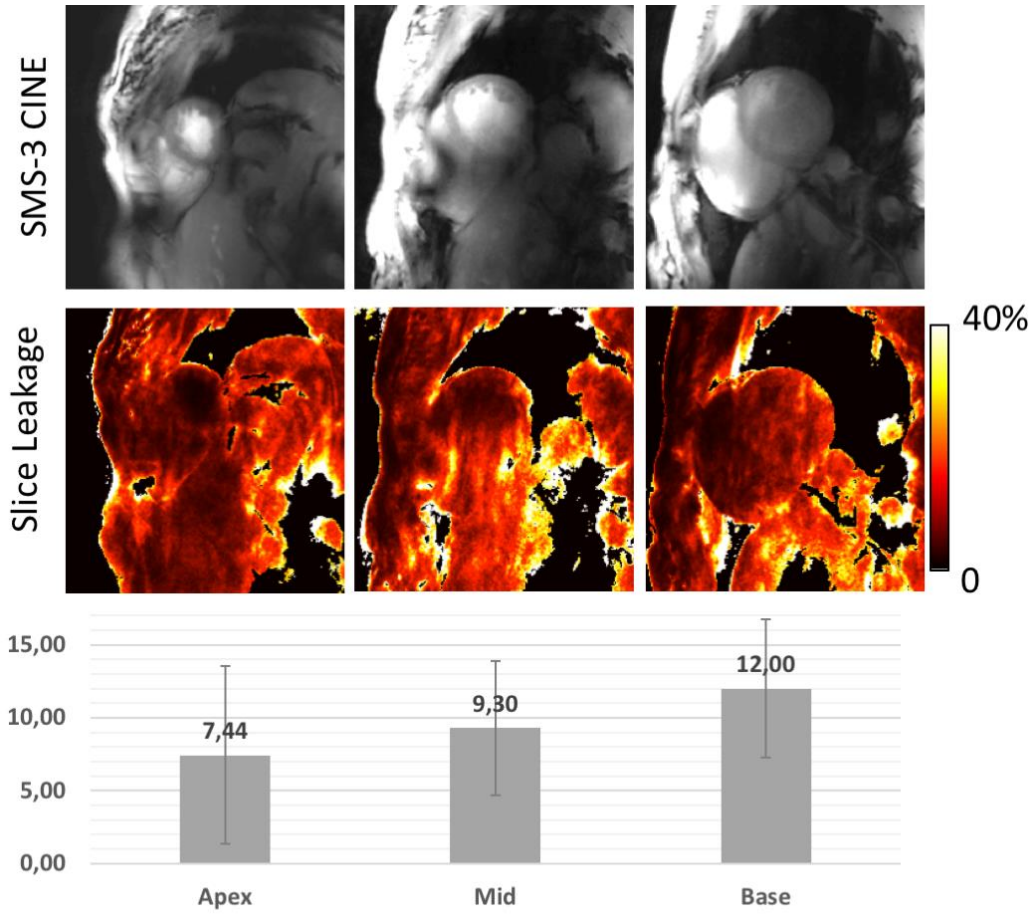

Figure 7: SMS slice leakage measured at the three levels of the ventricle showed increased leakage from apex to base. Leakage maps were masked for visualization. Average slice leakage measured in the left ventricle is reported in the graph below for all volunteers.

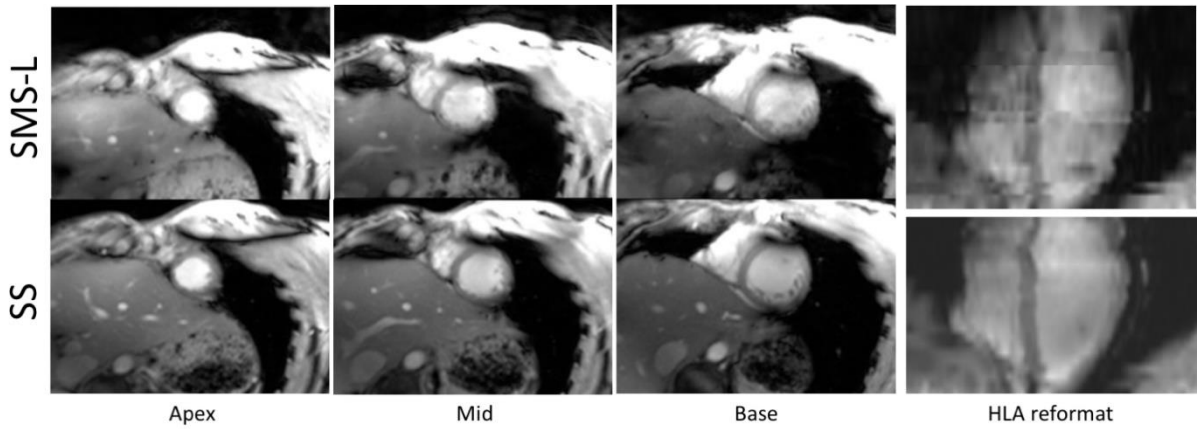

Figure 8: Short axis slices and horizontal long axis (HLA) reformat of the entire stack from the single-slice cine and the SMS-3-cine with SMS-L image reconstruction. Note that SMS-3 cine covers the lower part of the atria as well due to the fixed slice gap in this study.

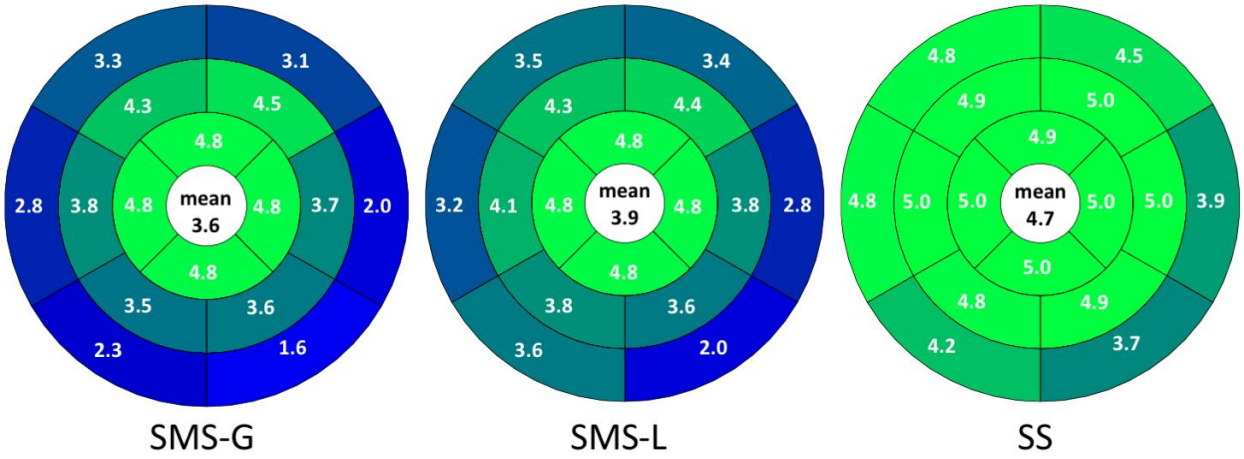

Figure 9: Bullseye plots of quality assessment of myocardium wall visualization and contractile function for the 16 left ventricle segments. Even with SS, the posterior segments of the basal slice were sometimes difficult to observe throughout the cardiac cycle. SMS-G and SMS-L suffered from severe loss of signal and contrast particularly at the basal level.

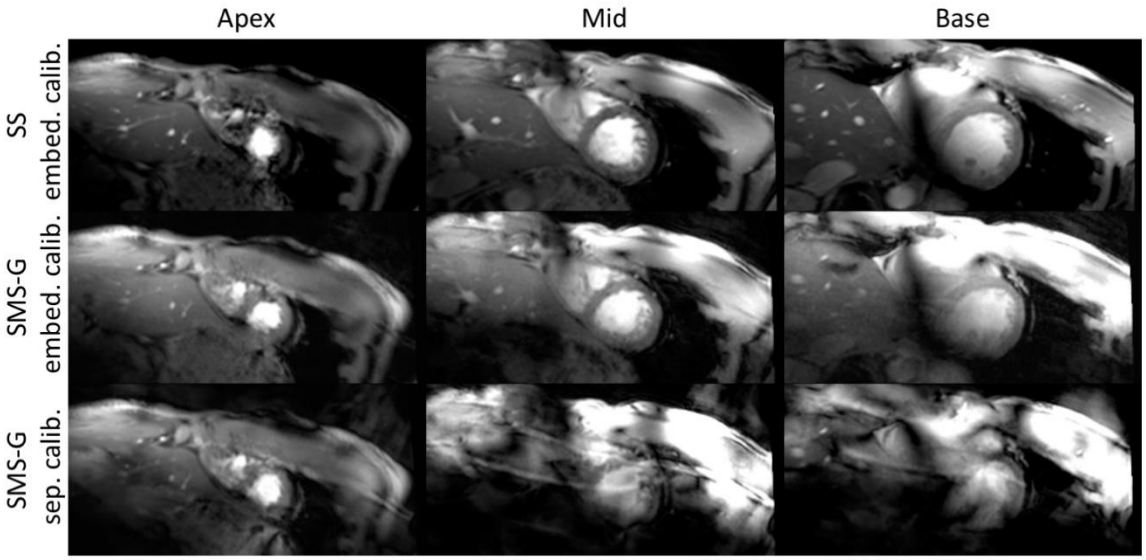

Figure 10: Comparison of SS and SMS-G with separate calibration or with proposed embedded Fourier-encoded calibration. The separate calibration data were acquired too early in the breath-hold, leading to mis-registration with the imaging data, thus the SMS reconstruction fails. Embedding the calibration data within the imaging dataset solves this issue.

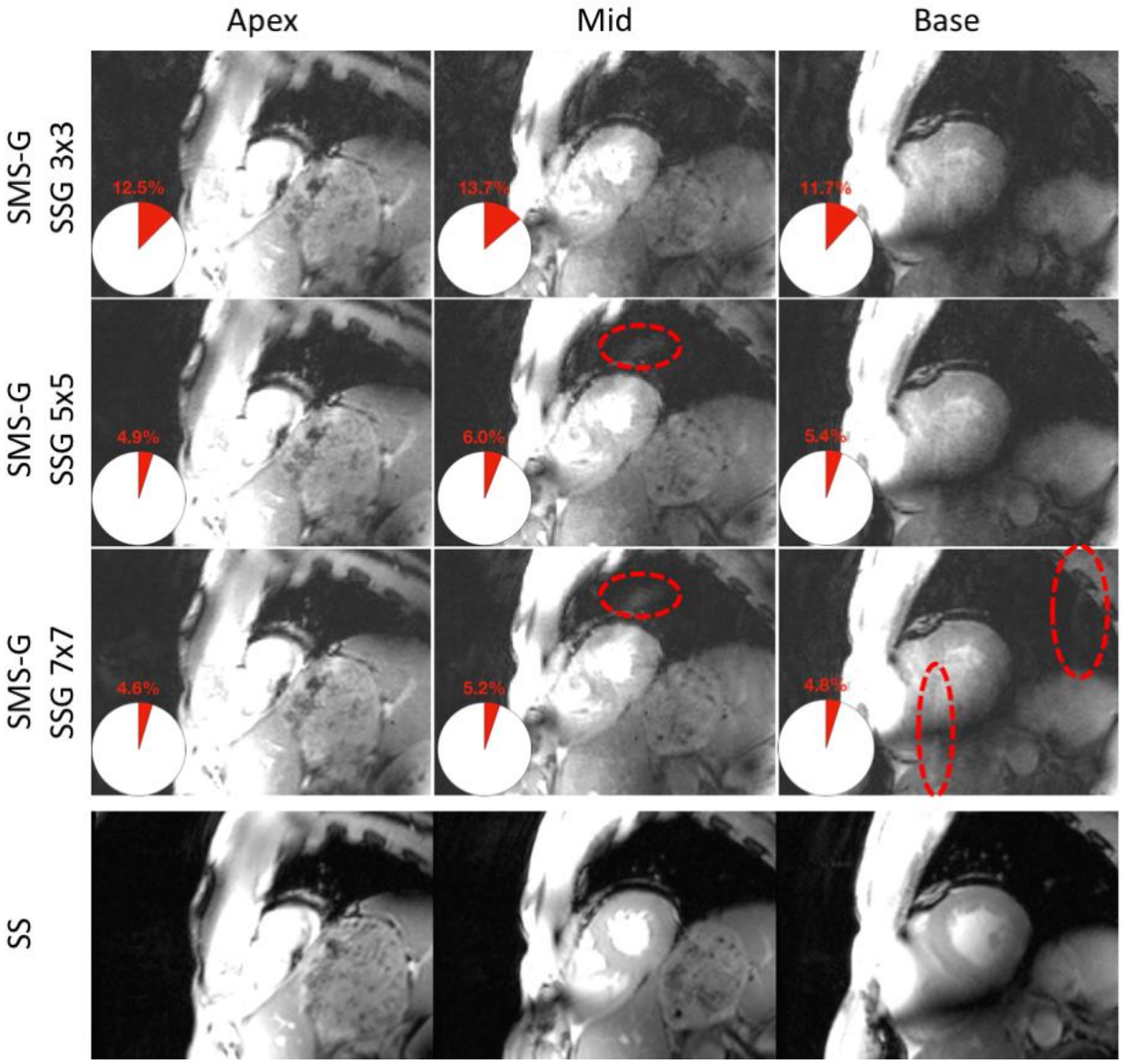

Supporting Information Figure S1: SMS-G reconstruction using increasing SSG kernel sizes from 3x3 to 7x7. Aliasing artifacts can be observed when the kernel size increases (red ellipses). The more conservative kernel size of 3x3 was chosen for this study to limit these artifacts.

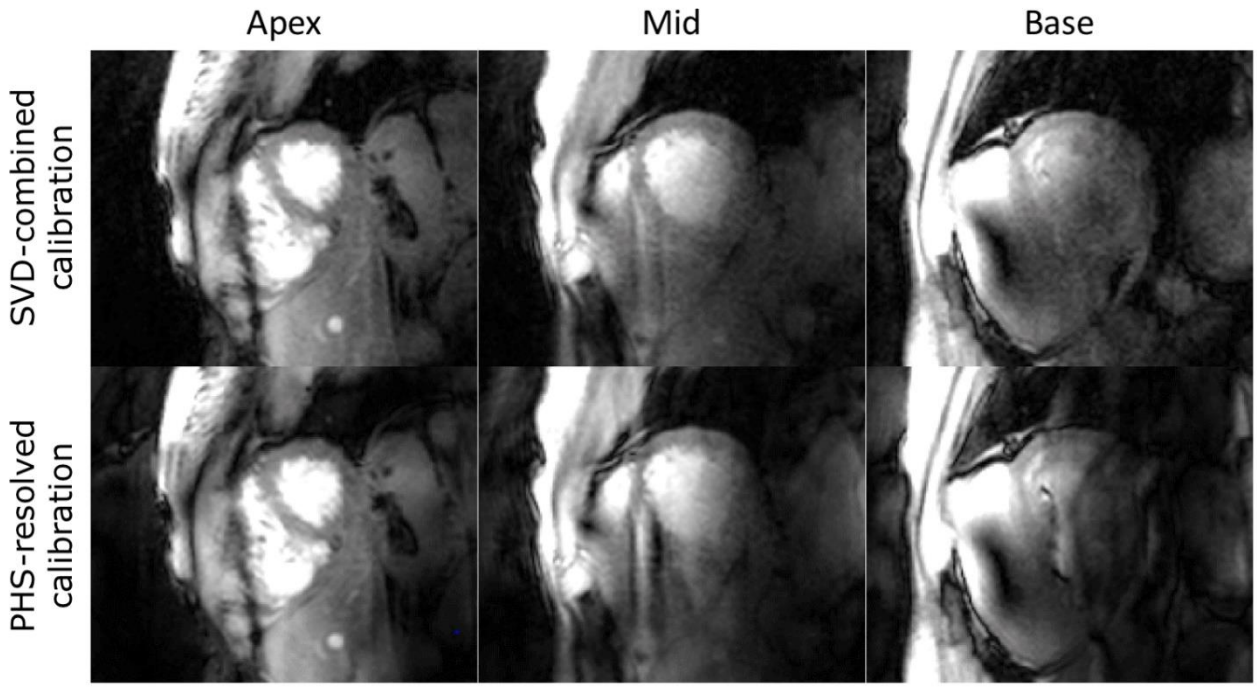

Supporting Information Figure S2: Comparison of the SMS reconstruction either using the combination of the multiple calibration datasets with singular value decomposition (SVD) or using calibration synchronous to the imaging datasets (phase-resolved). For the phase-resolved SMS calibration, each imaging cardiac phase is reconstructed using the nearest calibration dataset in cardiac time. This approach limits the influence of cardiac motion into the SMS reconstruction. However, in our study design, the individual calibration datasets were too noisy to robustly calibrate the SMS reconstruction.

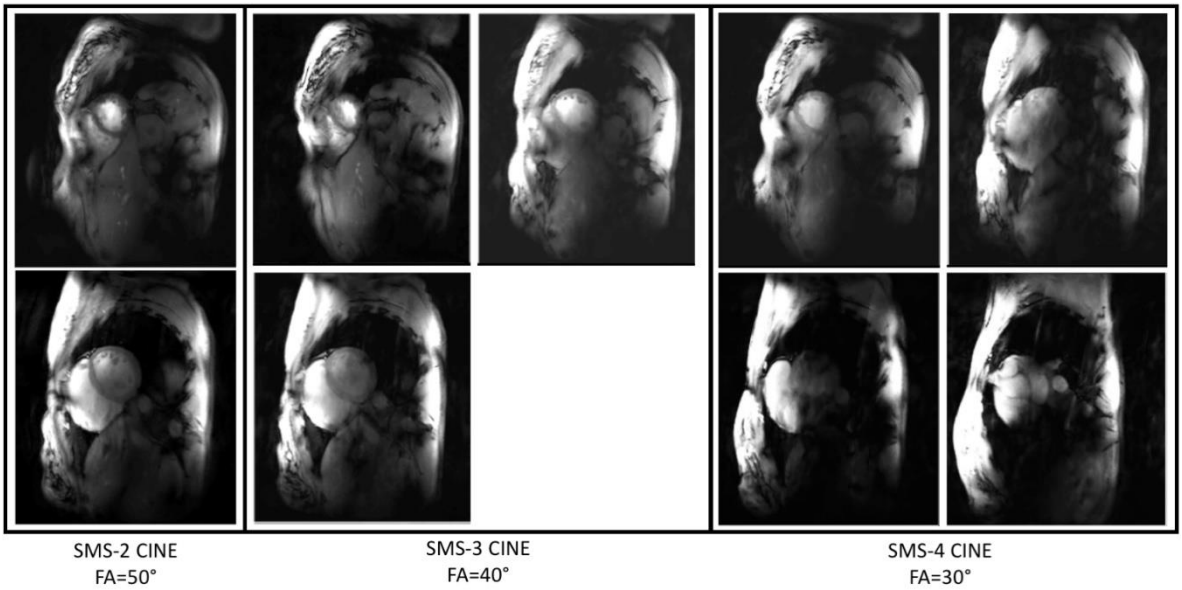

Supporting Information Figure S3: Example of results from SMS-2, SMS-3 and SMS-4 cine. SAR restrictions limited the increasing RF power of the SMS excitation pulses such that nominal flip angles (FA) decreased dramatically with increasing number of slices. As a consequence, SNR dropped severely for SMS-4 and image reconstruction (SMS-L) retained aliasing artifacts.